Recent Progress in Exact and Reduced-Order Modeling of Light-Scattering Properties of Complex Structures

Xu Li, *Member, IEEE*, Allen Taflove, *Fellow, IEEE*, and Vadim Backman

***Abstract*—An emerging research area in biophotonics with potentially near-term clinical applications in early stage cancer detection involves the investigation of possible correlations of the elastic light scattering properties of tissues with alterations in their cellular composition and nanostructure. Until recently, exploring these correlations has been impeded by a lack of robust and accurate mathematical models of the light scattering properties of complex structures. In this paper, we review recent progress in this area. Topics include: 1) development of accurate reduced-order expressions for the total scattering cross section spectra of a wide range of nonspherical and inhomogeneous particles; 2) rigorous finite-difference time-domain modeling results showing how the backscattering of light can be sensitive to nanometer scale features embedded within micrometer-scale particles; and 3) development of accurate reduced-order expressions for the backscattering depolarization properties of a wide range of inhomogeneous particles. These advances provide an improved science base for cellular level biophotonics, and have promise to accelerate the development of novel corresponding clinical technologies.**

***Index Terms*—Cancer diagnosis, finite difference time domain (FDTD), light-scattering spectroscopy, scattering.**

I. Introduction

DURING the past decade, it has become apparent that the analysis of the elastic light scattering characteristics of living tissue can provide valuable diagnostic information. Preliminary data has suggested that alteration in these light scattering signatures may be used as a sensitive marker to detect neoplasia at an earlier stage than possible by histological analysis, where some crucial information may be lost due to tissue fixing, staining, and the limited resolution of microscopes [1]. A number of techniques, such as elastic light-scattering spectroscopy [1]–[5], angle-resolved low coherence interferometry [6], [7], and the recently proposed coherent backscattering spectroscopy [8], have been developed to exploit the elastic light scattering properties of tissue for disease diagnosis. In general, these techniques do not focus on providing a spatial map of the macroscopic optical properties of the tissue under test. Instead, they seek to detect minute cellular physiological differences, such as those between normal and cancerous/preinvasive cells, by examining the changes in spectral, angular, and polarization characteristics of light scattered from tissue. By providing information about tissue and cellular structures on the micro/nano scales, light scattering based techniques may offer improved diagnostic sensitivity in living tissue. This realization has motivated increased interest in utilizing elastic light scattering as a diagnostic mechanism, and incorporating the scattering features into traditional imaging based approaches to enhance their accuracy and sensitivity. Representative recent developments include optical coherence tomography enhanced by spectroscopic analysis [9] and static light scattering microscopy [10].

For any technique relying on elastic light scattering as a diagnostic mechanism, data analysis and correlation of the light scattering properties of tissues with alterations in their cellular composition and nanostructure plays an essential role in the diagnostic process. Conventionally, the interpretation of measured data involves extracting the size, refractive index, and density of tissue structures such as cell nuclei and other organelles by comparing the observed scattering features with Mie theory, which is an analytical solution of light scattering by homogeneous spherical particles. This approach has been demonstrated to be a powerful tool to provide quantitative information on cellular structures [2], [11]. However, this approach clearly relies upon the approximation of the cellular scattering particles as homogeneous spheres. This approximation cannot account for the complexity of the structures of biological tissue. Furthermore, it cannot account for the subtle and complex cellular changes during the initial onset of the malignancy, including changes in the morphology and internal texture characteristics of the nuclei and organelles.

In order to fully utilize the potential of elastic light scattering for disease diagnosis, it is important to understand the mechanism by which changes in shape and internal structure of nuclei and cell organelles affect light scattering. This understanding will provide researchers with fundamental insights regarding the means to improve techniques and data analysis methods to maximize diagnostic sensitivity and accuracy. For example, it is important to know which tissue properties can or cannot be determined by use of light scattering. From a clinical standpoint, if certain measures of the light scattering signal from tissues can be unambiguously and reliably associated with disease-specific cellular changes, this knowledge will facilitate the development

Manuscript received December 31, 2004; revised August 4, 2005. This work was supported by the National Science Foundation under Grants BES-0238903 and ACI-0219925. The computational resource was provided by the NSF Teragrid under Project TG-MCB 040062N.

X. Li is with the Department of Biomedical Engineering and the Department of Electrical Engineering and Computer Science, Northwestern University, Evanston, IL 60208 USA (e-mail: xuli@northwestern.edu).

A. Taflove is with the Department of Electrical Engineering and Computer Science, Northwestern University, Evanston, IL 60208 USA (e-mail: taflove@ece. northwestern.edu).

V. Backman is with the Department of Biomedical Engineering, Northwestern University, Evanston, IL 60208 USA (e-mail: v-backman@northwestern.edu).

Digital Object Identifier 10.1109/JSTQE.2005.857691

and acceptance of optical methods for screening and diagnosis of patients and for preclinical/basic biological studies.

Recent advancements in numerical methods of solving Maxwell's equations have made it possible to calculate light scattering by inhomogeneous objects of arbitrary shape and internal organization. In particular, the application of the finite-difference time-domain (FDTD) method [12] has yielded fruitful results in modeling light scattering by individual cells [13]–[15]. However, significant computational resources required by the FDTD method, or other exact numerical solutions of Maxwell equations for arbitrary geometries, do not allow for the calculation of light scattering by macroscopic tissue structures. The large computational requirement also poses a significant challenge in utilizing exact modeling to address the inverse problem, wherein multiple solutions of the forward problem are often required. A more feasible approach to calculate light scattering by complex tissue structure is to combine numerical modeling with reduced-order analytical models.

In this paper, we review recent progress in both exact numerical modeling and reduced-order analytical approximations for light scattering by particles with complex shapes and internal structure. Our objective here is to provide an overview of relevant principles, techniques, and current research by coherently integrating the body of published work with new results. In Section II, we introduce two stochastic models, the Gaussian random sphere (GRS) model and the Gaussian random field (GRF) model, for describing and synthesizing irregular shapes and internal structures. These geometric models provide test beds for the subsequent theoretical development. Section III presents the development of an accurate reduced-order expression, the equiphase-sphere (EPS) approximation, for the total scattering cross section (TSCS) spectra of a variety of nonspherical and inhomogeneous particles. We demonstrate that a wide range of particles with subwavelength perturbations in their shapes or internal inhomogeneities have TSCS spectra similar to their equiphase-sphere counterparts. In Section IV, we present FDTD modeling results demonstrating that the backscattering of light can be sensitive to nanometer-scale features within the particles. Finally, Section V presents the development of a reduced-order expression for the backscattering depolarization properties of inhomogeneous particles.

II. Stochastic Methods for Modeling the Geometry of Nonspherical and Inhomogeneous Particles

In order to investigate light scattering by particles with a wide variety of shapes and interior structures, statistical approaches are very useful for modeling the particle geometry [16]. This is especially the case for investigating light scattering by biological tissues, wherein shape irregularities and internal inhomogeneities exist at a wide range of length scales. In this section, we introduce two stochastic models, the Gaussian random sphere (GRS) model to synthesize nonspherical shapes, and Gaussian random field (GRF) model to synthesize inhomogeneous internal textures.

The GRS model [16] is defined in spherical coordinates as having angle-dependent radius $r(\vartheta, \varphi)$ with mean radius $r_0 =$

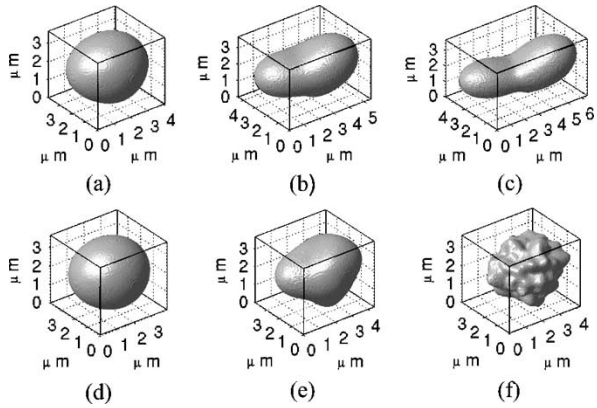

Fig. 1. Examples of Gaussian random spheres with fixed $r_0 = 1.75$ μm. (a)–(c) Gaussian spheres with increasing δ_r (Γ is fixed at 70°). (d)–(f) Gaussian spheres with decreasing Γ (δ_r is fixed at 0.1). (a) $\delta_r = 0.1, \Gamma = 70°$, (b) $\delta_r = 0.5, \Gamma = 70°$, (c) $\delta_r = 0.9, \Gamma = 70°$, (d) $\delta_r = 0.1, \Gamma = 90°$, (e) $\delta_r = 0.1, \Gamma = 30°$, (f) $\delta_r = 0.1, \Gamma = 10°$.

$\langle r(\vartheta, \varphi) \rangle$ and normalized standard deviation of the radius $\delta_r = \sqrt{\langle (r(\vartheta, \varphi) - R)^2 \rangle}/r_0$. Using a modified Gaussian correlation function, the correlation between two radii over solid angle Ω is

$$C_r(\Omega) = \exp\left(-\frac{\sin^2(\Omega/2)}{2\sin^2(\Gamma/2)}\right) \tag{1}$$

where Γ is the correlation angle of the Gaussian sphere, defined as the angular displacement over which the correlation drops to $1/\sqrt{e}$. The shape characteristics of a Gaussian random sphere are uniquely determined by the statistical parameters r_0, δ_r, and Γ.

We generate the three-dimensional (3-D) geometry of Gaussian spheres using a computer program based on the code developed by Muinonen and Nousiainen [17]. As shown in Fig. 1(a)–(c), increasing δ_r results in an increased deformation of the particle shape from a sphere. On the other hand, as illustrated in Fig. 1(d)–(f), reducing Γ leads to increased short-distance fluctuations (increased numbers of "valleys" and "hills") on the particle surface.

Similarly, the GRF model [18] mathematically describes a random process having a Gaussian probability density function. Here, we consider the refractive index $n(\boldsymbol{r})$ as a function of spatial location $\boldsymbol{r} = (x, y, z)$. Each value of $n(\boldsymbol{r})$ is a Gaussian random variable with mean $n_0 = \langle n(\boldsymbol{r}) \rangle$ and normalized standard deviation $\delta_n = \sqrt{\langle (n(\boldsymbol{r}) - n_0)^2 \rangle}/(n_0 - 1)$. For a GRF distribution with Gaussian function as the correlation model, the two-point correlation function $C_n(r)$ is given by

$$C_n(r) = e^{-r^2/(L_c/2)^2} \tag{2}$$

where L_c is the characteristic correlation length representing the length scale over which the correlation drops to a negligible level. For such choice of correlation function, the characteristics of the spatial distribution of $n(\boldsymbol{r})$ are determined by n_0, δ_n, and L_c.

Using the turning-band method [19], we create geometrical models of spherical particles with refractive index having GRF distributions. Fig. 2 shows graphs of six representative particles with refractive index distributions synthesized by the GRF

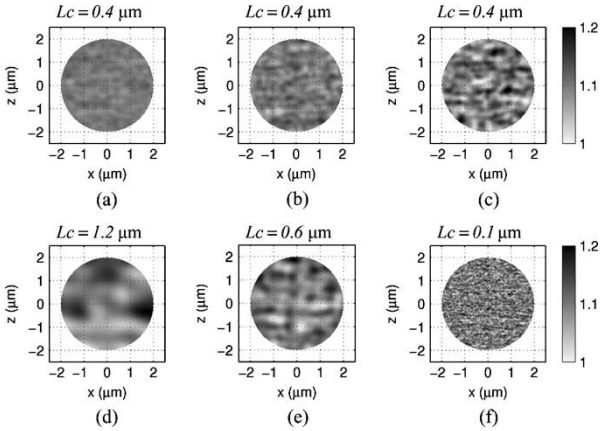

Fig. 2. Examples of inhomogeneous spherical particles having GRF refractive-index distributions with fixed $n_0 = 1.1$ and $r_0 = 2$ μm. The $\hat{\mathbf{x}} - \hat{\mathbf{z}}$ cross sectional cuts of the particles' interior refractive-index distribution are mapped in grayscale. (a)–(c) Inhomogeneous particles with increasing δ_n (L_c is fixed at 0.4 μm). (d)–(f) Inhomogeneous particles with decreasing L_c (δ_n is fixed at 0.2). (a) $\delta_n = 0.12, Lc - 0.4$ μm, (b) $\delta_n = 0.24, Lc - 0.4$ μm, (c) $\delta_n = 0.32, Lc - 0.4$ μm, (d) $\delta_n = 0.2, Lc - 1.2$ μm, (e) $\delta_n = 0.2, Lc - 0.6$ μm, (f) $\delta_n = 0.2, Lc - 0.1$ μm.

model. In each example, we map the $\hat{\boldsymbol{x}} - \hat{\boldsymbol{z}}$ cross sectional cut of the particle's interior refractive index distribution in grayscale. In Fig. 2(a)–(c), L_c is fixed at 0.4 μm while δ_n increases from 0.12 [Fig. 2(a)] to 0.32 [Fig. 2(c)]. In Fig. 2(d)–(e), δ_n is fixed at 0.2 while L_c decreases from 1.2 μm [Fig. 2(d)] to 0.1 μm [Fig. 2(f)]. These examples demonstrate the capability of the GRF model to mimic refractive index fluctuations occurring over a variety of geometrical scales. It is evident that δ_n describes the magnitude of refractive index variability, while L_c characterizes the size of the internal features of the particle.

Figs. 1 and 2 demonstrate that stochastic models such as GRS and GRF are capable of representing complex shapes and internal structures spanning a wide range of length scales which are characteristic to cellular structures. These geometries are also mathematically well parameterized, and thus are suitable to serve as test beds for generalized theoretical development. In our subsequent analyses and numerical experiments, we use these geometries as generic representation of a wide range of nonspherical and inhomogeneous geometries.

III. Development of Accurate Reduced-Order Expressions for the Total Scattering Cross Section Spectra of Nonspherical and Inhomogeneous Particles—the EPS Approximation

The total scattering cross section (TSCS) is one of most important parameters describing the light scattering properties of particles. For a homogeneous sphere, the TSCS can be readily calculated with Mie theory for any wavelength. For particles with irregular shapes and internal structures, however, no exact analytical solution is available to characterize the wavelength dependence of their TSCS. For such particles, approximation methods are desirable for providing practical solutions to light-scattering problems. Our investigation has been focused on particles with sizes in the resonance range (on the order of a few wavelengths). Light scattering by particles within this size range exhibits complicated dependencies on wavelength and scattering angles, and cannot be characterized by Rayleigh or Rayleigh–Gans approximations. Such particles are also of great relevance to tissue optics, since many structures such as cell nuclei are in this size range.

We have recently introduced the equiphase-sphere (EPS) approximation for calculating the TSCS spectra of nonspherical [20], [21] and inhomogeneous particles [22]. In the EPS approximation, the wavelength dependent TSCS spectrum of a particle is given by the sum of the "edge effect" term $\sigma_s^{(s)}(\lambda)$ and "volume diffraction effect" term $\sigma_s^{(v)}(\lambda)$ [23], [24]

$$\sigma_s(\lambda) = \sigma_s^{(s)}(\lambda) + \sigma_s^{(v)}(\lambda). \tag{3}$$

Here, $\sigma_s^{(s)}(\lambda)$ can be approximated as [23]

$$\sigma_s^{(s)}(\lambda) \approx 2S[2\pi(3V/4\pi^{1/3}/\lambda]^{-2/3} \tag{4}$$

where S is the particle's maximum cross section area transverse to the direction of the incident light, and V is the volume of the particle.

Based on the Wentzel–Kramers–Brillouin (WKB) technique, we approximate the volume term $\sigma_s^{(v)}(\lambda)$ as [20], [22]

$$\sigma_s^{(v)}(\gamma) = 2S[1 - 2n_0 \sin\rho/\rho + 4n_0 \sin^2(\rho/2)/\rho^2] \tag{5}$$

where n_0 is the volume averaged refractive index and $\rho = 2\pi d(n_0 - 1)/\lambda$ is the maximum phase-shift produced by the "equiphase sphere" of the particle. For a nonspherical particle, the equiphase sphere is defined as the "best-fitting" ellipsoid of the particle. We note that finding the best-fitting ellipsoid for an arbitrary 3-D shape is generally a multiparameter optimization problem with eight free parameters: three semiaxes (a, b, and c); three coordinates of the center (x_0, y_0, and z_0); and two rotational angles (θ_0 and ϕ_0). Here, we fix some of these parameters to simplify the optimization procedure. First, we specify semiaxis c to be aligned with the incident wave vector $\hat{z}$. Thus we have $\theta_0 = 0$. The second constraint is to match the cross section area of the ellipsoid with the projected area of the particle in the $\hat{x} - \hat{y}$ plane ($S_p = \pi\, a\, b$). Furthermore, the location of the geometric center (x_0, y_0, z_0) is assigned to the center of mass of the irregular particle. Therefore, we need to determine only three free parameters: the longitudinal semiaxis c, the aspect ratio of the cross section $\eta_T = a/b$, and the transverse rotational angle ϕ_0 (the angle between cross section major semiaxis a and $\hat{x}$). The objective of the optimization procedure is to minimize the mean squared difference of the $\hat{z}$-directed light ray pathlength between the irregular particle and the corresponding ellipsoid. Parameters η_T, c, and ϕ_0 are chosen such that

$$\arg(c, \eta_T, \phi_0)\big|_{\min\{\langle \|\delta L_r\|^2 \rangle\}}. \tag{6}$$

After finding its best fitting ellipsoid and volume averaged refractive index, the TSCS spectrum of the irregularly shaped particle is then approximated by (3)–(5), where $d = 2c$.

In order to apply the EPS method in practice, it is important to determine the range of validity of this approximation. Also,

based on the WKB technique, we have derived the validity conditions of the EPS approximation as functions of the statistical parameters of the particle geometry and internal structures. For an inhomogeneous spherical particle with diameter $2r_0$, normalized refractive index standard deviation δ_n, and correlation length L_c, the validity condition of the EPS approximation is given by

$$\beta_n \equiv 4\sqrt{2r_0}\,(n_0-1)\sqrt{L_c}\delta_n/\lambda < 1. \tag{7}$$

Similarly, we have determined the range of validity of the EPS approximation for particles with irregular shapes. For a nonspherical particle radial standard deviation Δ from its best fitting ellipsoid and radius-angular correlation angle Γ, the validity condition of the EPS approximation is given by

$$\beta_r \equiv 2\sqrt{2/\pi}(n_0-1)\sqrt{\Gamma}\Delta/\lambda < 1. \tag{8}$$

We note from (7) and (8) that two effects contribute to the validity and accuracy of the EPS approximation for inhomogeneous and nonspherical particles: 1) the magnitude of the perturbation in the shape or the inhomogeneity of the particle, represented by Δ and $\delta_n\,(n_0-1)$ respectively; and 2), the geometrical scale of the surface or internal features, denoted by Γ and L_c. The fact that β is proportional to Γ and L_c indicates that when inhomogeneity or surface irregularity occurs on length scales that are small compared to the incident wavelength, they have less impact on the validity of the EPS approximation. In other words, particles with smaller-scale perturbations in their shapes or internal inhomogeneities have similar TSCS spectra as their equiphase-sphere counterparts. This effect can be observed from Figs. 3 and 4, where we compare the TSCS spectra calculated by the EPS approximation with accurate FDTD benchmark data for a variety of nonspherical and inhomogeneous particles. These examples also demonstrate that the EPS approximation (3)–(5) are capable of modeling the TSCS spectra for a wide range of nonspherical and inhomogeneous particles when the validity conditions given by (3) and (4) are satisfied. Furthermore, the mathematical simplicity of these reduced-order expressions also makes them especially appealing for being applied in inverse-scattering problems [21].

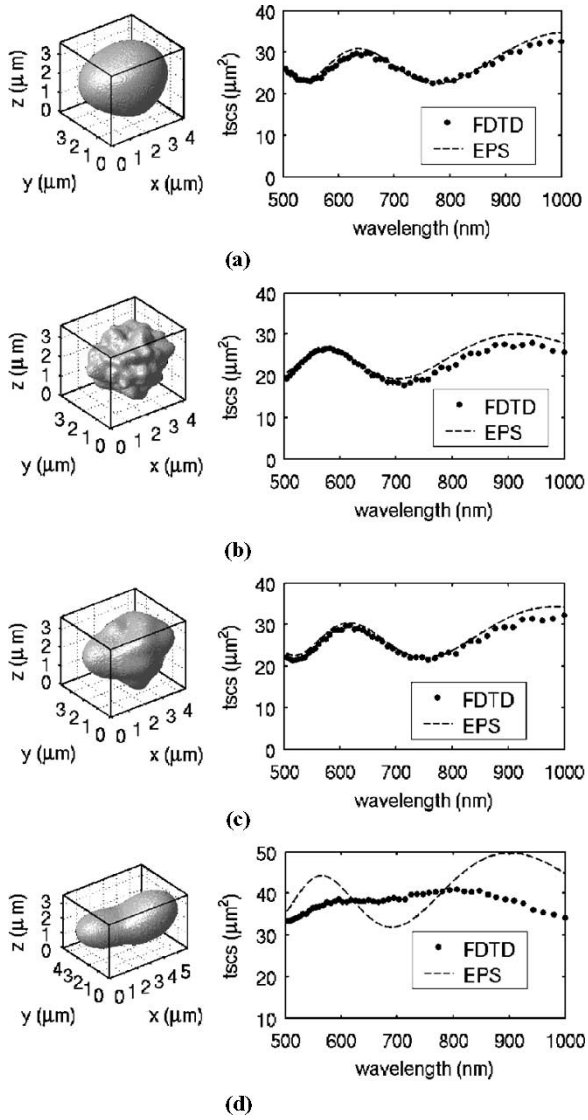

Fig. 3. Demonstration of the accuracy of EPS approximation applied to nonspherical particles. TSCS spectra calculated by EPS approximation are compared to FDTD benchmark data. The incident light propagates in the $\hat{z}$ direction. (a)–(c) Demonstration that when $\beta_r < 1$, the EPS approximation can give reasonable accuracy for calculating the TSCS spectra. (d) When $\beta_r > 1$, the validity of the EPS approximation is not guaranteed. (a) $\Delta = 0.3\ \mu$m, $\Gamma = 50^\circ, \bar{\beta}_r = 0.45$, (b) $\Delta = 0.7\ \mu$m, $\Gamma = 10^\circ, \bar{\beta}_r = 0.48$, (c) $\Delta = 0.6\ \mu$m, $\Gamma = 20^\circ, \bar{\beta}_r = 0.57$, (d) $\Delta = 0.8\ \mu$m, $\Gamma = 70^\circ, \bar{\beta}_r = 1.5$.

IV. Sensitivity of Backscattering Signatures to Nanoarchitecture of Scattering Structures

Our analysis and numerical examples, shown in Section III, indicates that the TSCS spectra of nonspherical and inhomogeneous dielectric particles are not sensitive to shape and texture perturbations at length scales much smaller than the wavelength. An important question then arises for researchers investigating optical tissue diagnostic techniques: are there any light-scattering parameters that provide sufficient sensitivity to detect nanometer-scale cellular changes? This question is of particular interest, since recent clinical evidence has indicated that light scattering signals are extremely sensitive to minute differences in tissue and cellular structures [1]. As we will discuss, contrary to the TSCS, light-scattering signals in the backward direction contain signatures that are sensitive to such nanoscale perturbations.

Here, we demonstrate the sensitivity of backscattering signatures to nanoscale parameters using the FDTD method. Prior to this investigation, we developed and validated a simple yet effective modification to significantly improve the accuracy of the FDTD near-to-far field (NTFF) transformation for calculating the backscattering of strongly forward-scattering objects [25]. We use the modified FDTD-NTFF approach to calculate the spectral and angular distribution of backscattered light from inhomogeneous dielectric particles with identical sizes and volume-averaged refractive indices, and compare the calculated scattering patterns with their homogeneous counterpart. This comparison is illustrated in the middle panels of Fig. 5, where we plot the scattering intensity distribution as

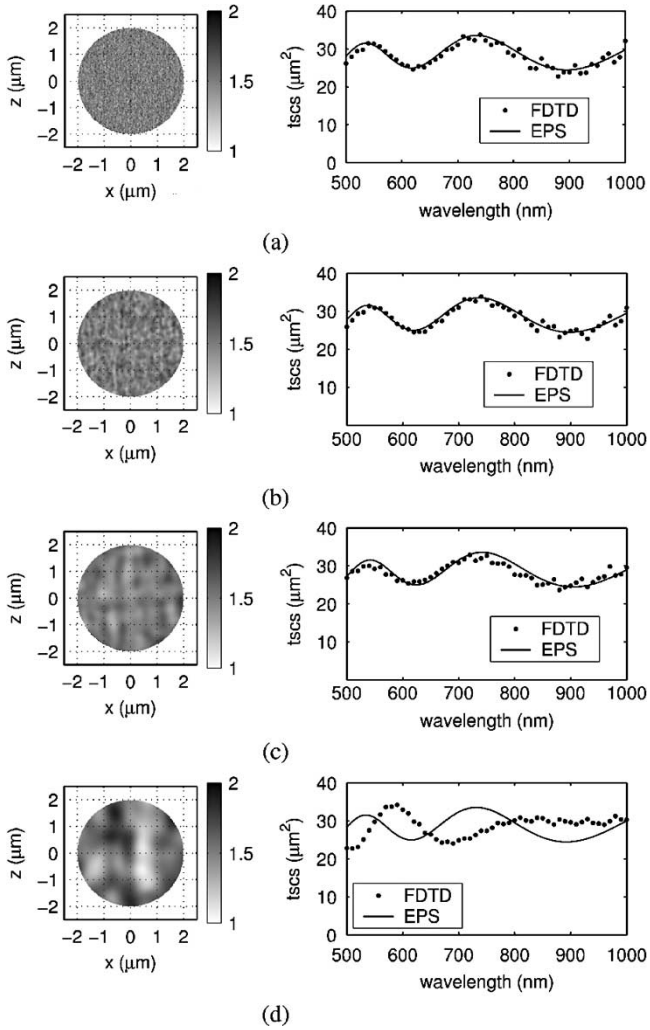

Fig. 4. TSCS spectra calculated using rigorous FDTD numerical modeling and EPS analyses for inhomogeneous particles. The Spatial distribution of the particle refractive index in the $\hat{x} - \hat{z}$ cross sectional cut is displayed in the left panel. (a)–(c) Demonstration that when $\beta_n < 1$, the EPS approximation can give reasonable accuracy for calculating the TSCS spectra. (d) When $\beta_n > 1$, the validity of the EPS approximation is not guaranteed. (a) $\delta_n = 0.2$, $Lc = 50$ nm, $\bar{\beta}_n = 0.36$, (b) $\delta_n = 0.16$, $Lc = 200$ nm, $\bar{\beta}_n = 0.57$, (c) $\delta_n = 0.16$, $Lc = 600$ nm, $\bar{\beta}_n = 0.98$, (d) $\delta_n = 0.32$, $Lc = 1000$ nm, $\bar{\beta}_n = 2.5$.

functions of wavelength and scattering angle (centered at the backscattering direction). Distinct scattering features are evident in the scattering fingerprints from the two inhomogeneous particles, although their inhomogeneities have characteristic sizes much smaller than the illumination wavelength ($L_c = 50$ and 100 nm, respectively, while $\bar{\lambda} = 750$ nm). These numerical results strongly support the hypothesis that there exit signatures in backscattered light that are sensitive enough to detect alterations in nanoscale architectures. Importantly, this sensitivity is not limited by the diffraction limit. Potentially, backscattering signatures can serve as biomarkers to detect and characterize slight alterations in tissue structure. For comparison, we also plot the scattering intensity distribution in the forward direction. Here, no distinct scattering features are observed among the different scatterers. The similarity in the forward scattering pattern is not surprising. For these strongly forward-scattering

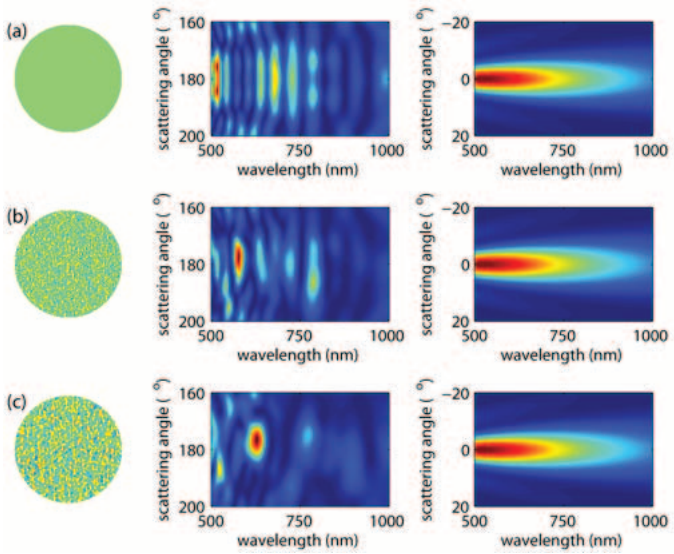

Fig. 5. Demonstration of the sensitivity of backscattering signatures to nanoarchitecture of scattering structures. The particle geometries are shown in the left panel. FDTD-calculated backscattering intensity distribution over wavelength and scattering angle are displayed in the middle panel. The forward scattering signatures are displayed in the right panel. All three particles have $n_0 = 1.1$ and $r_0 = 2$ μm. (a) Homogeneous particle. (b) Inhomogeneous particle with $Lc = 50$ nm}, $\delta_n (n_0 - 1) = 0.02$. (c) Inhomogeneous particle with $Lc = 100$ nm $\delta_n (n_0 - 1) = 0.02$.

particles, the forward and small angle scattering is the major contribution to the TSCS spectra, which are not sensitive to small scale structures, as shown in Section III.

V. Quantitative Analysis of Depolarization of Light Backscattering by Inhomogeneous Particles

In addition to spectral and angular properties, the polarization properties of light backscattered by biological tissue can also be used as diagnostically valuable markers. Recently, we have investigated the depolarization effect of dielectric particles having complex internal structures by examining the distribution of optical paths and the associated phase changes of light rays propagating in the particle [26]. Our theoretical analyses and numerical experiments demonstrate that the backscattered linear depolarization ratio is directly associated with the statistical parameters of the particle's internal geometry. Specifically, for an inhomogeneous particle having an internal refractive index distribution with standard deviation $\sigma_n = \delta_n (n_0 - 1)$ and correlation length L_c, the linear depolarization in the backscattered light $\delta_\lambda \equiv I_\perp / I_\parallel$ is given by

$$\delta_\lambda \approx C\,(2\pi/\lambda^2)(L_C \sigma_n)^2 \tag{9}$$

where C is a constant independent of the distribution of the internal refractive index.

Fig. 6 shows three representative results of our numerical experiments where backscattered intensities in both polarizations ($I_\parallel$ and $I_\perp$) are calculated for inhomogeneous particles. Ignoring the oscillatory structures due to resonances in the backscattered spectra, it is clear that the overall level of $I_\perp$, and therefore the

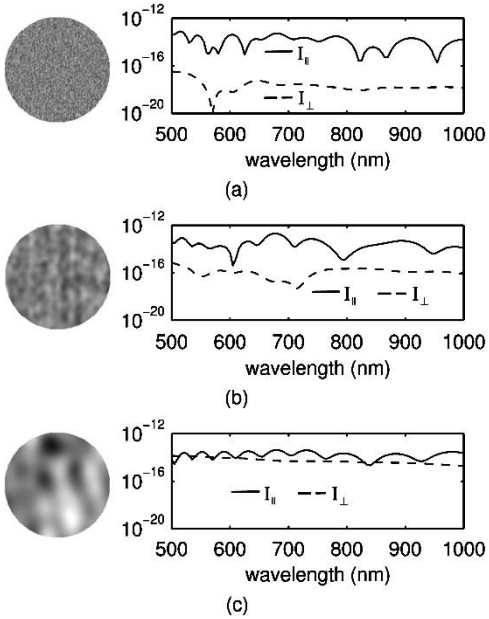

Fig. 6. Demonstration that the overall intensity of cross-polarized backscattering light increases as $L_c\sigma_n$ becomes greater. Here, copolarized and cross-polarized backscattering light intensity calculated by FDTD method for inhomogeneous dielectric spheres with $n_0 = 1.1, r_0 = 2\ \mu$m, and a variety of L_c and σ_n. (a) $L_c = 0.05\ \mu$m, $\sigma_n = 0.02$; (b) $L_c = 0.4\ \mu$m, $\sigma_n = 0.016$; (c) $L_c = 1.2\ \mu$m, $\sigma_n = 0.035$.

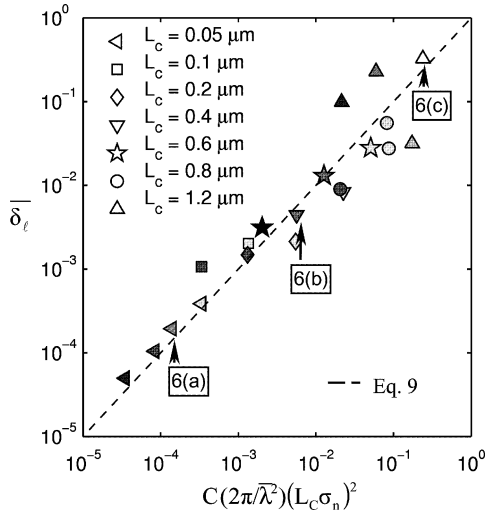

Fig. 7. Confirmation of the validity of (9); i.e., that δ_λ is approximately proportional to $(2\pi/\lambda)(\mathrm{L_C}\sigma_n)^2$. Here, averaged linear depolarization ratio are calculated from FDTD simulations conducted on 20 inhomogeneous dielectric spheres as a function of the geometrical parameter $\beta \equiv C\,(2\pi/\bar{\lambda}^2)(L_C\,\sigma_n)^2$ with L_c ranging from 0.05 to 1.2 μm, and σ_{n} ranging from 0.005 to 0.035. In the calculation of β, we choose $C = 12$ and $\bar{\lambda} = 750$ nm. The grayscale level of each data point represents the magnitude of σ_n with the brighter shades corresponding to greater σ_{n}s.

linear depolarization ratio δ_λ, increases as the product of L_c and σ_n becomes larger.

The dependence of δ_λ on the geometric characteristics of the particle's internal refractive-index distribution is most evident in Fig. 7, where we summarize our numerical experiments conducted on 20 inhomogeneous dielectric spheres with L_c ranging from 0.05 μm to 1.2 μm and σ_n ranging from 0.005 to 0.036. Here, we graph δ_λ averaged over the 500–1000 nm incident wavelength range against the geometric parameter $\bar{\beta} \equiv C(2\pi/\bar{\lambda}^2)(L_C\sigma_n)^2$ in a log-log plot to cover a wide range for both parameters. The constant C is chosen empirically as $C = 12$ to give the best linearity. The 20 data points are plotted with symbols representing different L_c and grayscale levels corresponding to different σ_n for each particle geometry. We also cross reference three data points with their corresponding backscattered spectra shown in Figs. 6(a)–(c). The relationship given in (9) is plotted in dashed line to compare against the data points. The reasonable data fitting confirms the validity of (9); i.e., that δ_λ is proportional to $(L_C\sigma_n)^2/\lambda^2$ for the first order of approximation.

VI. Summary and Discussion

In this paper, we have reviewed recent progress in analytical and numerical modeling of light scattering by particles having complex shapes and internal structures. We have introduced stochastic geometric descriptions, namely the Gaussian random sphere (GRS) and the Gaussian random field (GRF) models, for characterizing and synthesizing irregular shapes and internal structures in a wide range of length scales which are characteristic of cellular structures. Using these model geometries as test beds, we have developed a reduced-order expression, the EPS approximation, for calculating the TSCS spectra of complex shapes. We have also developed a reduced-order expression to quantitatively analyze the depolarization of light backscattering by inhomogeneous particles. These analytical approximations have simple mathematical forms, and thus can be use to address the inverse problem to extract certain geometrical parameters of the scatterers from measured scattering data.

The validity range of the EPS approximation indicates that a variety of particles with subwavelength perturbations in their shapes or internal inhomogeneities have TSCS spectra similar to their equiphase-sphere counterparts. However, as demonstrated by our FDTD numerical modeling, there exist scattering signatures in backscattered light that are sensitive to nanometer-scale features embedded within micron-scale particles. These results substantiate previous experimental observations that backscattered light signals may be used to detect minute changes in cellular structures occurring in the early stage of carcinogenesis.

The advances presented in this paper may provide an improved science base for cellular-level biophotonics, and have promised to accelerate the development of novel corresponding clinical technologies by providing insights on the correlations of the elastic light scattering properties of tissues with alterations in their cellular composition and nanostructure.

Acknowledgment

X. Li would like to thank Dr. Y. L. Kim and Y. Liu for helpful discussions on elastic light scattering for tissue diagnosis.

REFERENCES

[1] H. K. Roy, Y. Liu, R. K. Wali, Y. L. Kim, A. K. Kromin, M. J. Goldberg, and V. Backman, "Four-dimensional elastic light-scattering fingerprints as preneoplastic markers in the rat model of colon carcinogenesis," *Gastroenterology*, vol. 126, pp. 1071–1081, 2004.

[2] V. Backman, M. B. Wallace, L. T. Perelman, J. T. Arendt, R. Gurjar, M. G. Muller, Q. Zhang, G. Zonios, E. Kline, T. McGillican, S. Shapshay, T. Valdez, K. Badizadegan, J. M. Crawford, M. Fitzmaurice, S. Kabani, H. S. Levin, M. Seiler, R. R. Dasari, I. Itzkan, J. Van Dam, and M. S. Feld, "Detection of preinvasive cancer cells," *Nature*, vol. 406, no. 6791, pp. 35–36, 2000.

[3] J. R. Mourant, T. M. Johnson, S. Carpenter, A. Guerra, T. Aida, and J. P. Freyer, "Polarized angular dependent spectroscopy of epithelial cells and epithelial cell nuclei to determine the size scale of scattering structures," *J. Biomed. Opt.*, vol. 7, no. 3, pp. 378–387, 2002.

[4] Y. L. Kim, Y. Liu, R. K. Wali, H. K. Roy, M. J. Goldberg, A. K. Kromin, K. Chen, and V. Backman, "Simultaneous measurement of angular and spectral properties of light scattering for characterization of tissue microarchitecture and its alteration in early precancer," *IEEE J. Sel. Topics Quantum Electron.*, vol. 9, no. 2, pp. 243–256, Mar./Apr. 2003.

[5] L. B. Lovat, K. Johnson, M. R. Novelli, M. O'Donovan, S. Davies, C. R. Selvasekar, S. Thorpe, I. J. Bigio, and S. G. Bown, "Optical biopsy using elastic scattering spectroscopy can detect high grade dysplasia and cancer in Barrett's esophagus," *Gastroenterology*, vol. 126, no. 4, pp. A22–A22, 2004.

[6] A. Wax, C. H. Yang, M. G. Muller, R. Nines, C. W. Boone, V. E. Steele, G. D. Stoner, R. R. Dasari, and M. S. Feld, "In situ detection of neoplastic transformation and chemopreventive effects in rat esophagus epithelium using angle-resolved low-coherence interferometry," *Cancer Res.*, vol. 63, no. 13, pp. 3556–3559, 2003.

[7] J. W. Pyhtila, R. N. Graf, and A. Wax, "Determining nuclear morphology using an improved angle-resolved low coherence interferometry system," *Opt. Express*, vol. 11, no. 25, pp. 3473–3484, 2003.

[8] Y. L. Kim, Y. Liu, V. M. Turzhitsky, H. K. Roy, R. K. Wali, and V. Backman, "Coherent backscattering spectroscopy," *Opt. Lett.*, vol. 29, no. 16, pp. 1906–1908, 2004.

[9] D. C. Adler, T. H. Ko, P. R. Herz, and J. G. Fujimoto, "Optical coherence tomography contrast enhancement using spectroscopic analysis with spectral autocorrelation," *Opt. Express*, vol. 12, no. 22, pp. 5487–5501, 2004.

[10] A. K. Popp, M. T. Valentine, P. D. Kaplan, and D. A. Weitz, "Microscopic origin of light scattering in tissue," *Appl. Opt.*, vol. 42, no. 16, pp. 2871–2880, 2003.

[11] L. T. Perelman, V. Backman, M. Wallace, G. Zonios, R. Manoharan, A. Nusrat, S. Shields, M. Seiler, C. Lima, T. Hamano, I. Itzkan, J. Van Dam, J. M. Crawford, and M. S. Feld, "Observation of periodic fine structure in reflectance from biological tissue: A new technique for measuring nuclear size distribution," *Phys. Rev. Lett.*, vol. 80, p. 627, 1998.

[12] A. Taflove and S. Hagness, *Computational Electrodynamics: The Finite-Difference Time-Domain Method*. 3rd ed. Boston, MA: Artech, 2005.

[13] A. Dunn and R. Richards-Kortum, "Three-dimensional computation of light scattering from cells," *IEEE J. Sel. Topics Quantum Electron.*, vol. 2, no. 4, pp. 898–905, Dec. 1996.

[14] R. Drezek, A. Dunn, and R. Richards-Kortum, "ight scattering from cells: Finite-difference time-domain simulations and goniometric measurements," *Appl. Opt.*, vol. 38, no. 16, pp. 3651–3661, 1999.

[15] D. Arifler, M. Guillaud, A. Carraro, A. Malpica, M. Follen, and R. Richards-Kortum, "Light scattering from normal and dysplastic cervical cells at different epithelial depths: Finite-difference time-domain modeling with a perfectly matched layer boundary condition," *J. Biomed. Opt.*, vol. 8, no. 3, pp. 484–494, 2003.

[16] K. Muinonen, "Light scattering by stochastically shaped particles," in *Light Scattering by Nonspherical Particles: Theory, Measurements, and Applications*, M. I. Mishchenko, J. W. Hovenier, and L. D. Travis, Eds. San Diego, CA: Academic, 2000.

[17] K. Muinonen and T. Nousiainen, *G-Sphere*, available under the GNU General Public License, 2002, http://www.meteo.helsinki.fi/~tpnousia/gsphere/index.html [Online].

[18] R. J. Adler, *The Geometry of Random Fields*. New York: Wiley, 1981.

[19] A. T. A. Wood and G. Chan, "Simulation of stationary Gaussian processes in [0, 1]," *J. Comput. Graph. Stat.*, vol. 3, no. 4, pp. 409–432, 1994.

[20] X. Li, Z. Chen, A. Taflove, and V. Backman, "Equiphase-sphere approximation for analysis of light scattering by arbitrarily-shaped nonspherical particles," *Appl. Opt.*, vol. 43, no. 23, pp. 4497–4505, 2004.

[21] X. Li, Z. Chen, J. Gong, A. Taflove, and V. Backman, "Analytical techniques for addressing forward and inverse problems of light scattering by irregularly shaped particles," *Opt. Lett.*, vol. 29, no. 11, pp. 239–1241, 2004.

[22] X. Li, Z. Chen, A. Taflove, and V. Backman, "Equiphase sphere approximation for light scattering by stochastically inhomogeneous particles," *Phy. Rev. E*, vol. 70, pp. 056611–056618, 2004.

[23] Z. Chen, A. Taflove, and V. Backman, "Equivalent volume-averaged light scattering behavior of randomly inhomogeneous dielectric spheres in the resonant range," *Opt. Lett.*, vol. 28, no. 10, pp. 765–767, 2003.

[24] Z. Chen, A. Taflove, and V. Backman, "Concept of the equiphase sphere for light scattering by nonspherical dielectric particles," *J. Opt. Soc. Amer. A*, vol. 21, no. 1, pp. 88–97, 2004.

[25] X. Li, A. Taflove, and V. Backman, "Modified FDTD near-to-far field transformation for improved backscattering calculation of strongly forward-scattering objects," *IEEE Antennas Wireless Propag. Lett.*, vol. 4, no. 1, pp. 35–38, 2005.

[26] X. Li, A. Taflove, and V. Backman, "Quantitative analysis of the depolarization of backscattered light by stochastically inhomogeneous dielectric particles," *Opt. Lett.*, vol. 30, no. 8, pp. 902–904, 2005.

Xu Li (S'99–M'03) received the M.S. degree in biomedical engineering in 2000 and the Ph.D. degree in electrical and computer engineering in 2003, both from the University of Wisconsin-Madison.

From 2003 to 2005, she was a Postdoctoral Fellow and subsequently a Research Associate in the Department of Biomedical Engineering, Northwestern University, Evanston, IL. She is now an Assistant Professor in the Department of Biomedical Engineering and the Department of Electrical and Computer Engineering, Northwestern University. Her research interests include computational and experimental electromagnetics, microwave imaging and sensing techniques for biomedical applications, biophotonics, and electrodynamics of nanophotonic devices.

Allen Taflove (F'90) received the B.S., M.S. and Ph.D. degrees in electrical engineering from Northwestern University, Evanston, IL, in 1971, 1972, and 1975, respectively.

He has been a Professor in the Department of Electrical and Computer Engineering, Northwestern University since 1984. Since 1972, he has pioneered basic theoretical approaches and engineering applications of finite difference time domain computational electrodynamics. He coined the FDTD acronym in a 1980 IEEE paper, and in 1990 was the first person to be named a Fellow of the IEEE in the FDTD area. He has authored or co-authored five books, 20 book chapters and articles, over 100 refereed journal papers and 300 conference papers, and 14 U.S. patents. He has been the adviser or co-advisor of 20 Ph.D. recipients and one postdoctoral fellow, five of whom (including four women) are now tenured or tenure-track university professors. He is currently an elected member of Northwestern's General Faculty Committee, and is the graduate program Chair of his department. He is also the faculty advisor to the Undergraduate Design Competition, the Honors Program in Undergraduate Research, and the student chapters of Eta Kappa Nu and Tau Beta Pi. His efforts on behalf of students at all levels were recognized by Northwestern in 2000, when he was named a Charles Deering McCormick Professor of Teaching Excellence. His research interests span much of the electromagnetic spectrum.

Vadim Backman received the Ph.D. degree in medical engineering and medical physics from Harvard University and the Massachusetts Institute of Technology, Cambridge, MA, in 2001.

He is an Assistant Professor of biomedical engineering at Northwestern University, Evanston, IL. His research interests include biomedical optics, spectroscopy, development of theoretical approaches to describe light propagation in biological media, and optical diagnostic imaging.